ADVANCED FUNCTIONAL MATERIALS
www.afm-journal.de

Unraveling Mechanoluminescent Mechanisms in Doped CaZnOS Materials: Co-Mediation of Trap-Controlled and Non-Trap-Controlled Processes

*Wei Li, Yiyu Cai, Jianqing Chang, Shanshan Wang, Jianjun Liu, Lei Zhou, Mingmei Wu, and Jun-Cheng Zhang**

Doped CaZnOS materials show great potential for mechanoluminescence (ML) applications spanning the ultraviolet-visible-near infrared (UV–vis–NIR) range. However, conflicting reports regarding the generation and reproducibility of ML hinder the understanding and practical utilization of these materials. To address this issue, a comprehensive characterization strategy combining NIR laser-assisted de-trapping, UV irradiation-induced trap-filling, in situ mechanical stimulation, and continuous ML recording is proposed. Herein, the ML behaviors of four representative doped CaZnOS materials (Mn^{2+}, Bi^{3+}, Er^{3+}, and Ce^{3+}) are investigated using this approach. The results reveal that de-trapped materials exhibit non-trap-controlled ML, wherein ML intensity gradually weakens under successive mechanical stimuli without self-recovery. In contrast, trap-filled materials demonstrate both trap-controlled ML and non-trap-controlled ML, with the former predominantly contributing to the overall ML intensity. Notably, trap-controlled ML shows only partial recovery after trap filling. The non-trap-controlled ML is attributed to plastic ML and destructive ML phenomena, while explaining trap-controlled ML through the carrier de-trapping model. These results not only clarify conflicting reports but also provide clear insights into the ML properties and mechanisms of CaZnOS-based materials, facilitating advancements in practical applications. Furthermore, the developed characterization strategy is expected to serve as a valuable reference for establishing standardized protocols to evaluate ML performance.

1. Introduction

Mechanoluminescent materials have garnered significant attention due to their potential for converting external mechanical stimuli into light emission, offering promising applications in structural health diagnosis, lighting and displays, ultrasound-optogenetics, and human–computer interaction.[1–9] Among the various ML materials developed, CaZnOS-based materials stand out due to their unique capability to host diverse luminescent centers, enabling tunable ML spectra across the ultraviolet–visible–near infrared (UV–vis–NIR) range.[2,10,11] This versatility has demonstrated potential in colorful ML displays/sensors,[12–14] biomechanical imaging,[15,16] and biomedical light sources.[17,18] However, the reported ML properties and mechanistic interpretation of CaZnOS-based materials are highly contradictory, impeding their further development and utilization.

Previous studies have presented conflicting results regarding the generation and reproducibility of ML in CaZnOS-based materials, along with different understandings of the ML mechanisms (Table S1, Supporting Information). Some reports argued that UV irradiation was necessary for generating and reproducing ML. They observed that the ML intensity gradually decreased with continuous mechanical stimuli but could be fully or nearly fully restored by post-UV irradiation.[19–23] This phenomenon was explained by a trap-controlled ML model, wherein the cyclic process of carrier filling and de-trapping in traps governs the reproducibility of ML.[24–26] In contrast, another group of reports argued that ML can be generated

W. Li, Y. Cai, J. Chang, S. Wang, J. Liu, J.-C. Zhang
College of Physics and Optoelectronic Engineering
Faculty of Information Science and Engineering
Ocean University of China
Qingdao 266100, China
E-mail: zhangjuncheng@ouc.edu.cn

The ORCID identification number(s) for the author(s) of this article can be found under https://doi.org/10.1002/adfm.202305482

DOI: 10.1002/adfm.202305482

S. Wang, J. Liu, J.-C. Zhang
Engineering Research Center of Advanced Marine Physical Instruments and Equipment of Education Ministry of China
Key Laboratory of Optics and Optoelectronics of Qingdao
Ocean University of China
Qingdao 266100, China

L. Zhou, M. Wu
School of Chemical Engineering and Technology
Sun Yat-sen University
Zhuhai 519082, China

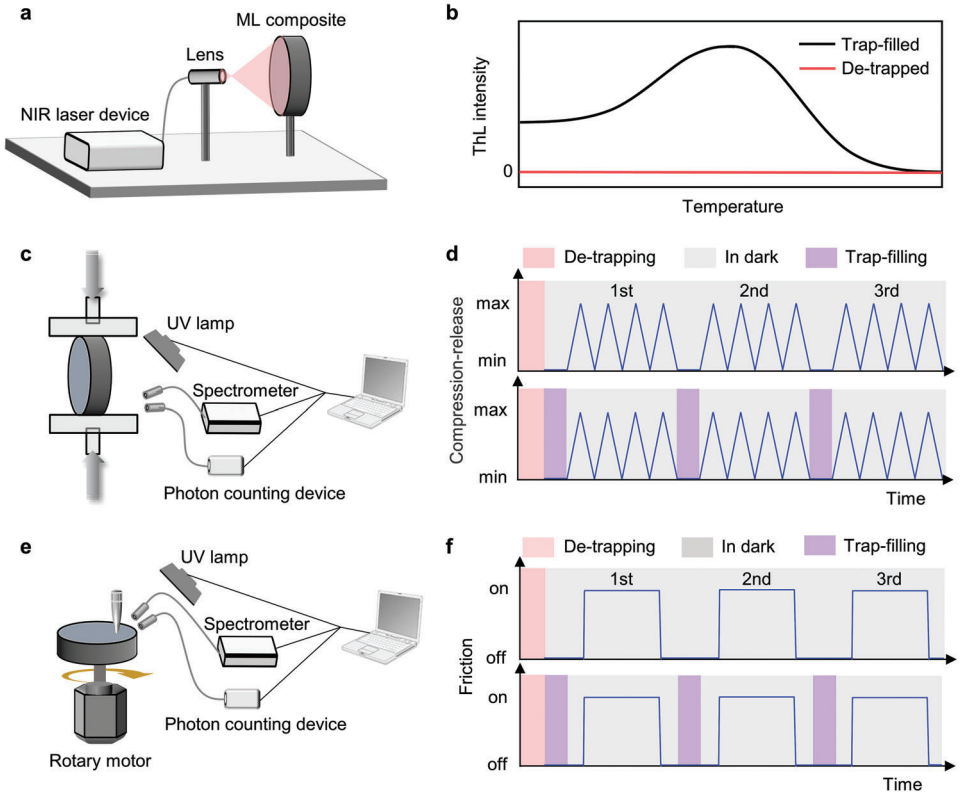

Scheme 1. Schematic diagrams illustrating the characterization of ML properties using NIR laser de-trapping-assisted in situ, real-time, and periodic testing. a) Experimental setup for de-trapping ML composites through irradiation with a NIR laser spot. b) Representative ThL curves showing the trap-filling process achieved by UV irradiation and subsequent de-trapping through NIR laser irradiation. c) Experimental setup for the collection of ML signals during in situ mechanical compression–release cycles. d) Design of periodic triangular wave loading for tests performed after de-trapping (top) and tests conducted after trap filling (bottom). e) Experimental setup for the collection of ML signals during cyclic circular friction. f) Design of periodic continuous friction for tests performed after de-trapping (top) and tests conducted after trap filling (bottom).

Table 1. Summarization of electron configuration, ML wavelength, and trap properties of four CaZnOS-based phosphors synthesized in this work.

Dopants	Electron configuration	Optical transition	ML peak [nm]	Trap density[a)]	Trap depth [eV]
Mn^{2+}	$3d^5$	$^4T_1$–$^6A_1$	620	0.33	0.66–0.81
Bi^{3+}	$6s^2$	$^3P_1$–$^1S_0$	485	100.00	0.64–0.91
Er^{3+}	$4f^{11}$	$^2H_{11/2}$–$^4I_{15/2}$	545	0.05	0.69–0.91
		$^4F_{9/2}$–$^4I_{15/2}$	660		
		$^4S_{3/2}$–$^4I_{13/2}$	850		
		$^4I_{13/2}$–$^4I_{15/2}$	1530		
Ce^{3+}	$4f^1$	$5d$–$^2F_{5/2}$,$^2F_{7/2}$	520, 570	5.00	0.66–0.85

[a)] Trap density: relative value derived from the integral intensity of ThL curves.

without UV irradiation and can maintain a stable output without significant decay under continuous mechanical stimuli,[27,28] a phenomenon referred to as self-recoverable ML.[29] This behavior was explained by a piezophotonic effect, wherein the piezoelectric effect separates polarization charges, leading to electron–hole recombination and ML generation.[30–32] Consequently, there is an urgent need for a comprehensive understanding of the ML performance and underlying mechanisms of CaZnOS-based materials.

Building on our previous work;[33–37] herein, we identify three possible reasons for the conflicting reports on the ML properties of CaZnOS-based materials. First, effectively eliminating trapped carriers in CaZnOS-based materials without altering the mechanical properties of the ML composites poses a significant challenge. These materials commonly contain carrier traps that can be charged by UV or ambient light sources such as sunlight and fluorescent lamps. To determine the necessity of pre-charging for ML generation, it is crucial to remove these trapped carriers. However, existing methods such as heat treatment, which empties the traps, often require high temperatures (up to 500 K).[38,39] Unfortunately, such temperatures can lead to the decomposition of the elastomeric polymers used in ML composite fabrication.[40,41] Consequently, the mechanical properties of the composites are altered, resulting in inaccurate ML characterization. Second, the lack of continuous in situ mechanical stimulation of the ML composites leads to an incorrect evaluation of ML reproducibility. Applying mechanical stimulation to different locations on the ML composite each time overlooks carrier de-trapping and ignores the potential structural damage caused by repeated and excessive mechanical stimulation. Last, many reports rely on integrated spectral data instead of transient photon

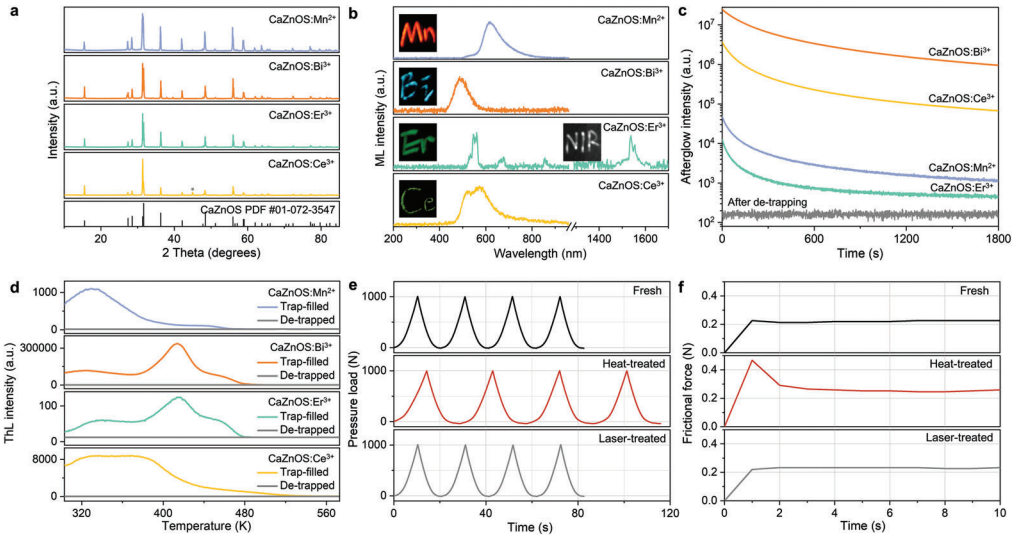

Figure 1. Structural and optical properties of doped CaZnOS phosphors and mechanical properties of prepared ML composites with and without NIR laser de-trapping. a) XRD patterns and b) ML spectra of the synthesized four phosphors. c) Afterglow curves and d) ThL curves of four phosphors after trap-filling with UV irradiation and subsequent de-trapping with NIR laser irradiation. e) Pressure load–time curves of fresh, heat-treated, and NIR laser-treated ML composites under a fixed triangular wave loading (1000 N, 3 mm min^{-1}). f) Frictional force–time curves of fresh, heat-treated, and laser-treated ML composites under a fixed continuous friction.

Table 2. Parameters of the mechanical stimulation employed to investigate the ML properties.

Materials	Compression–release cycle: maximum load, deformation rate		Cyclic friction: pressure, rotation speed	
	Condition 1	500 N, 3 mm min^{-1}	Condition 1	0.65 MPa, 2π rad s^{-1}
CaZnOS:Mn^{2+}/Bi^{3+}/Er^{3+}	Condition 2	1000 N, 3 mm min^{-1}	Condition 2	1.3 MPa, 2π rad s^{-1}
	Condition 3	1000 N, 5 mm min^{-1}	Condition 3	1.3 MPa, 4π rad s^{-1}
	Condition 2	1000 N, 3 mm min^{-1}	Condition 4	2.6 MPa, 4π rad s^{-1}
CaZnOS:Ce^{3+}	Condition 3	1000 N, 5 mm min^{-1}	Condition 5	3.9 MPa, 4π rad s^{-1}
	Condition 4	1500 N, 5 mm min^{-1}	Condition 6	3.9 MPa, 6π rad s^{-1}

signals to represent ML response.[15,19,23,27,28] This approach fails to capture the real-time response of ML to mechanical stimuli, potentially leading to mischaracterization of ML properties.

To address these challenges, in this study, we propose a comprehensive characterization strategy that integrates NIR laser-assisted de-trapping, in situ mechanical stimulation, and continuous recording of transient ML responses (**Scheme 1**). The NIR laser spot is used to evacuate the carrier traps in the CaZnOS-based phosphors and preserve the mechanical properties of the ML composites (Scheme 1a,b). In situ mechanical stimuli, including compression–release cycles and cyclic friction, are applied to the ML composites without changing their position throughout the ML test (Scheme 1c,e). Transient ML responses are captured using a photon counting system, enabling real-time monitoring of ML behavior. In addition, control experiments involving cyclic charging by UV irradiation are conducted to explore the influence of trap filling on ML properties. We meticulously design cyclic mechanical stimuli with varying parameters to systematically investigate ML properties (Scheme 1d,f). Subsequently, we analyze the obtained ML data and discuss the relevant ML mechanisms.

2. Results and Discussion

2.1. Material Preparation and NIR Laser De-Trapping

The CaZnOS host has the ability to incorporate various luminescent centers, including metals ions (Mn^{2+}, Cu^{2+}, and Bi^{3+}) and lanthanide ions (Ln^{3+} = Pr^{3+}, Nd^{3+}, Sm^{3+}, Eu^{3+}, Tb^{3+}, Dy^{3+}, Ho^{3+}, Er^{3+}, Tm^{3+}, and Yb^{3+}).[21,24,26,28] This study focuses on investigating the ML properties of doped CaZnOS materials using Mn^{2+}, Bi^{3+}, Er^{3+} and Ce^{3+}, as representative activators, chosen based on their characteristic emissions (**Table 1**). The phosphors were synthesized through a lithium-assisted solid-state reaction (see Experimental Section). The doping concentrations of Mn, Bi, and Er elements were selected based on the reported optimal values,[21,24,28] while the doping amount of Ce element was determined through an optimization experiment (Figure S1, Supporting Information). X-ray diffraction (XRD) patterns confirm the formation of the desired pure-phase structure (**Figure 1**a), with the sole exception of CaZnOS:Ce^{3+}, which exhibits a minor impurity phase of CaS. The presence of this impurity can be attributed to the use of a reducing atmosphere during the

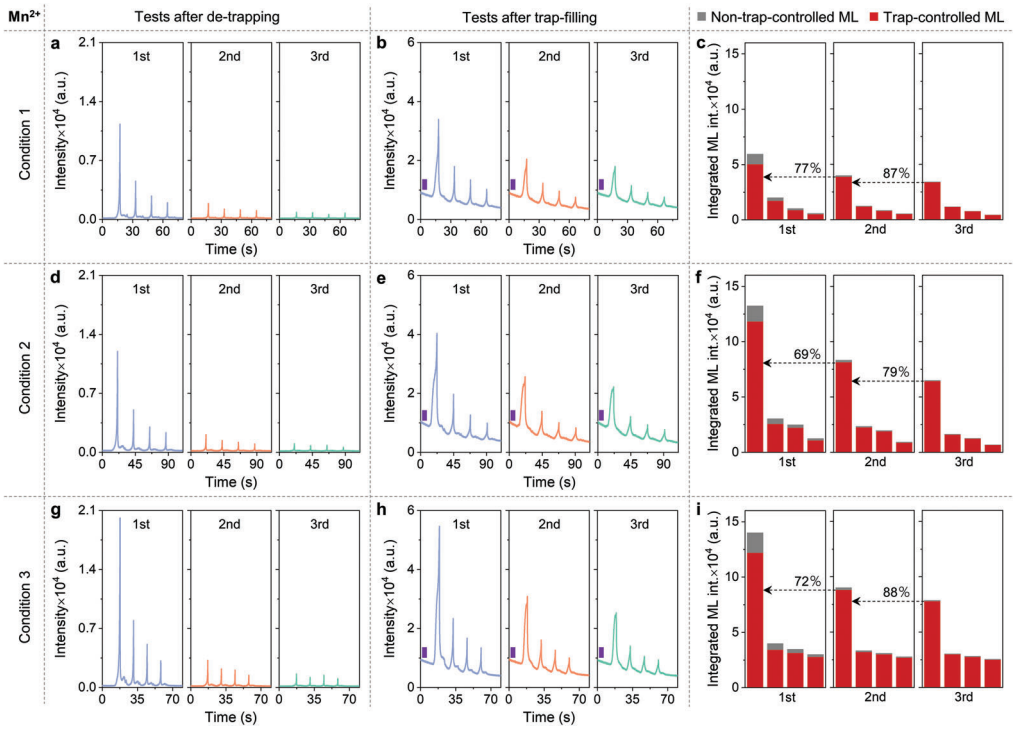

Figure 2. ML properties of CaZnOS:Mn^{2+} under compression–release cycles for different conditions. Panels a–c), d–f), and g–i) correspond to compression–release tests conducted under Condition 1, Condition 2, and Condition 3, respectively. Each panel includes: ML transient responses after de-trapping (a,d,g), ML transient responses after trap-filling (b,e,h), and derived intensities of non-trap-controlled ML and trap-controlled ML (c,f,i). Note: in (c,f,i), the arrows and percentage characters indicate the ratio of trap-controlled ML intensity after two adjacent UV irradiations.

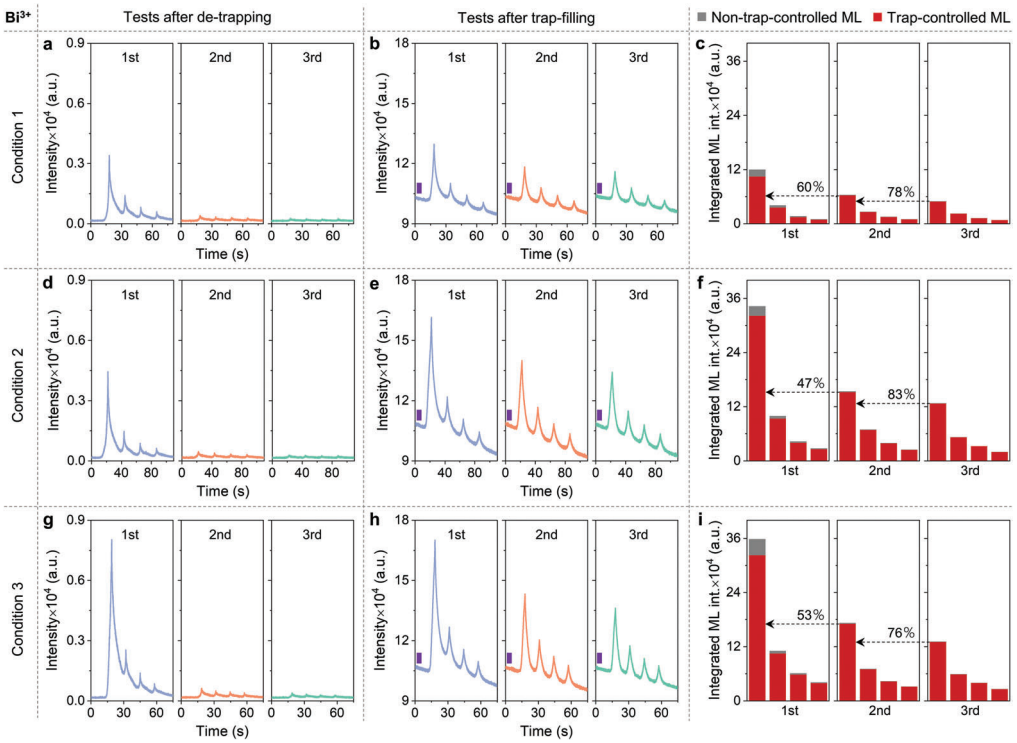

Figure 3. ML properties of CaZnOS:Bi^{3+} under compression–release cycles for different conditions. Panels a–c), d–f), and g–i) correspond to compression–release tests conducted under Condition 1, Condition 2, and Condition 3, respectively. Each panel includes: ML transient responses after de-trapping (a,d,g), ML transient responses after trap-filling (b,e,h), and derived intensity of non-trap-controlled ML and trap-controlled ML (c,f,i). Note: in (c,f,i), the arrows and percentage characters indicate the ratio of trap-controlled ML intensity after two adjacent UV irradiations.

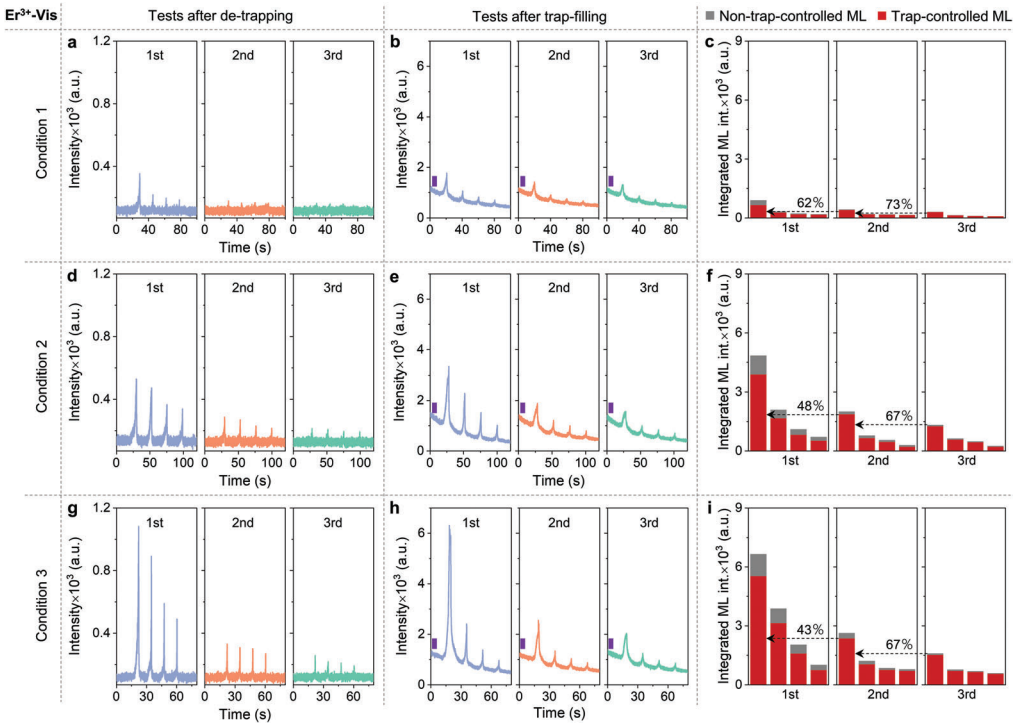

Figure 4. ML properties of CaZnOS:Er^{3+} at visible wavelengths under compression–release cycles for different conditions. Panels a–c), d–f), and g–i) correspond to compression–release tests conducted under Condition 1, Condition 2, and Condition 3, respectively. Each panel includes: ML transient responses after de-trapping (a,d,g), ML transient responses after trap-filling (b,e,h), and derived intensity of non-trap-controlled ML and trap-controlled ML (c,f,i). Note: in (c,f,i), the arrows and percentage characters indicate the ratio of trap-controlled ML intensity after two adjacent UV irradiations.

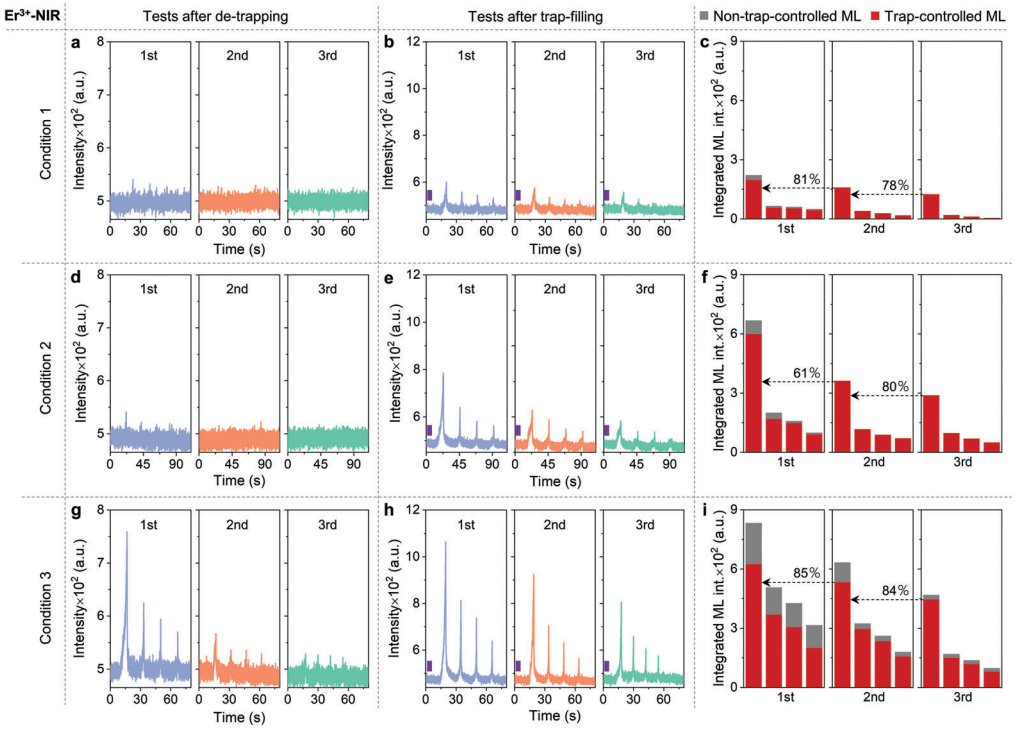

Figure 5. ML properties of CaZnOS:Er^{3+} at NIR wavelengths under compression–release cycles for different conditions. Panels a–c), d–f), and g–i) correspond to compression–release tests conducted under Condition 1, Condition 2, and Condition 3, respectively. Each panel includes: ML transient responses after de-trapping (a,d,g), ML transient responses after trap-filling (b,e,h), and derived intensity of non-trap-controlled ML and trap-controlled ML (c,f,i). Note: in (c,f,i), the arrows and percentage characters indicate the ratio of trap-controlled ML intensity after two adjacent UV irradiations.

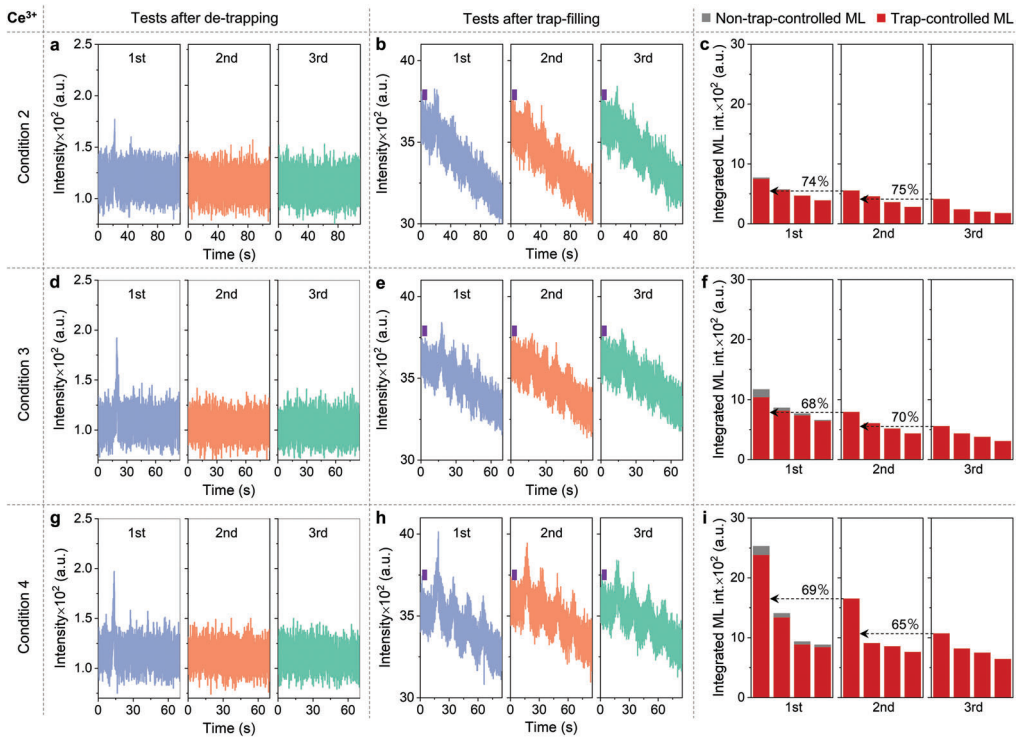

Figure 6. ML properties of CaZnOS:Ce^{3+} under compression–release cycles for different conditions. Panels a–c), d–f), and g–i) correspond to compression–release tests conducted under Condition 2, Condition 3, and Condition 4, respectively. Each panel includes: ML transient responses after de-trapping (a,d,g), ML transient responses after trap-filling (b,e,h), and derived intensity of non-trap-controlled ML and trap-controlled ML (c,f,i). Note: in (c,f,i), the arrows and percentage characters indicate the ratio of trap-controlled ML intensity after two adjacent UV irradiations.

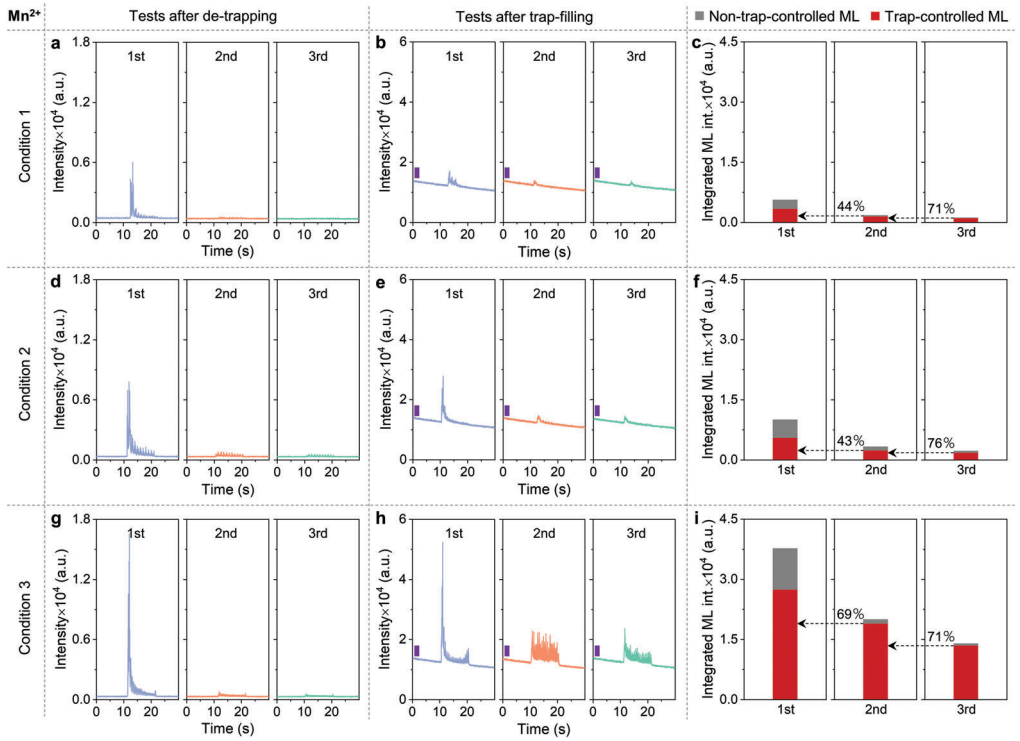

Figure 7. ML properties of CaZnOS:Mn^{2+} under cyclic friction tests for different conditions. Panels a–c), d–f), and g–i) correspond to compression–release tests conducted under Condition 1, Condition 2, and Condition 3, respectively. Each panel includes: ML transient responses after de-trapping (a,d,g), ML transient responses after trap-filling (b,e,h), and derived intensity of non-trap-controlled ML and trap-controlled ML (c,f,i). Note: in (c,f,i), the arrows and percentage characters indicate the ratio of trap-controlled ML intensity after two adjacent UV irradiations.

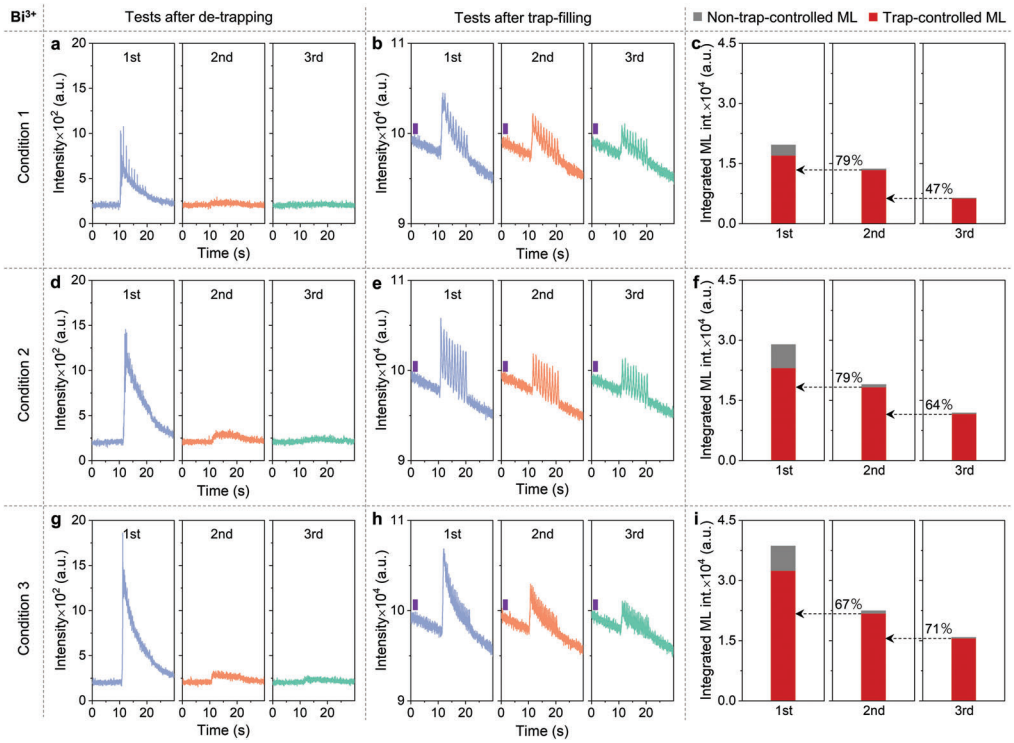

Figure 8. ML properties of CaZnOS:Bi^{3+} under cyclic friction tests for different conditions. Panels a–c), d–f), and g–i) correspond to compression–release tests conducted under Condition 1, Condition 2, and Condition 3, respectively. Each panel includes: ML transient responses after de-trapping (a,d,g), ML transient responses after trap-filling (b,e,h), and derived intensity of non-trap-controlled ML and trap-controlled ML (c,f,i). Note: in (c,f,i), the arrows and percentage characters indicate the ratio of trap-controlled ML intensity after two adjacent UV irradiations.

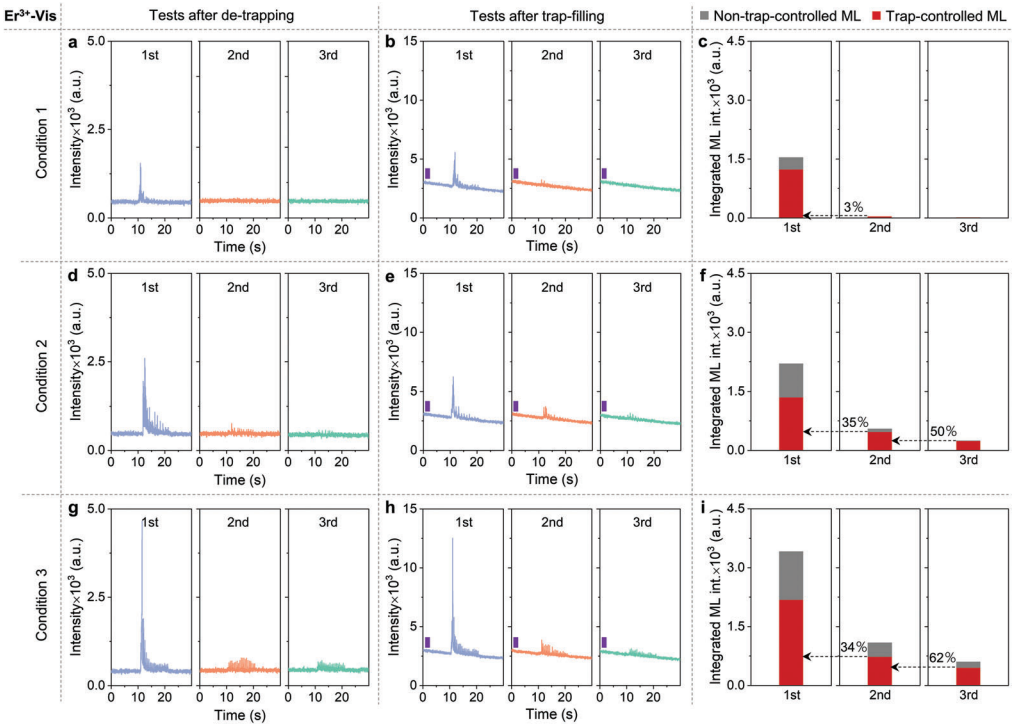

Figure 9. ML properties of CaZnOS:Er^{3+} at visible wavelengths under cyclic friction tests for different conditions. Panels a–c), d–f), and g–i) correspond to compression–release tests conducted under Condition 1, Condition 2, and Condition 3, respectively. Each panel includes: ML transient responses after de-trapping (a,d,g), ML transient responses after trap-filling (b,e,h), and derived intensity of non-trap-controlled ML and trap-controlled ML (c,f,i). Note: in (c,f,i), the arrows and percentage characters indicate the ratio of trap-controlled ML intensity after two adjacent UV irradiations.

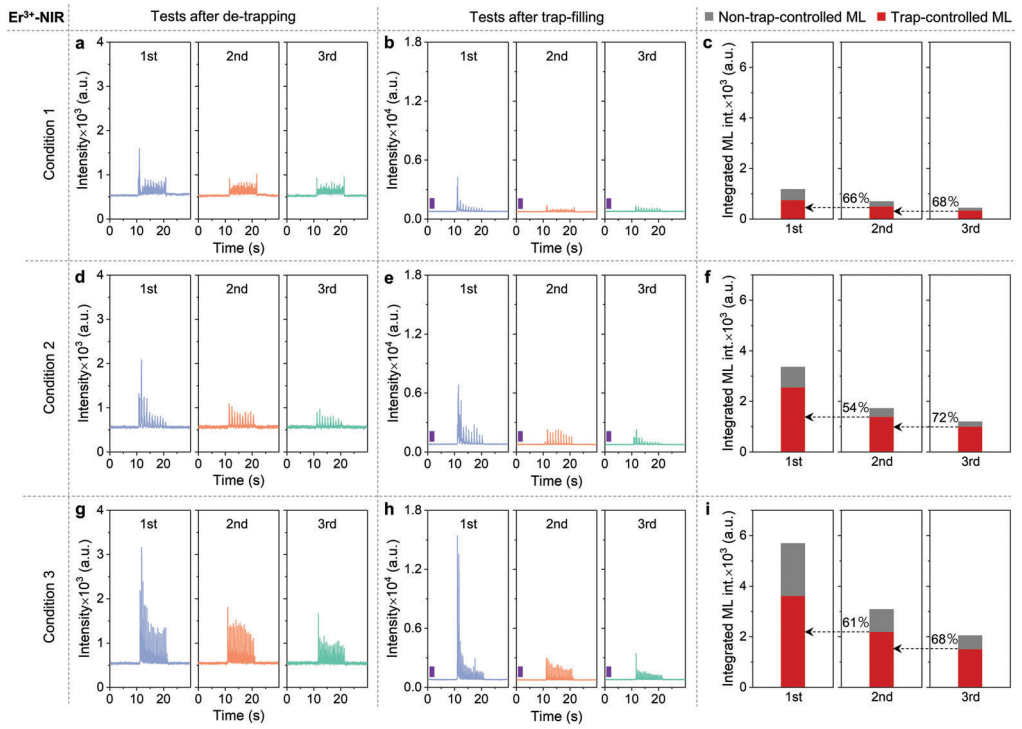

Figure 10. ML properties of CaZnOS:Er^{3+} at NIR wavelengths under cyclic friction tests for different conditions. Panels a–c), d–f), and g–i) correspond to compression–release tests conducted under Condition 1, Condition 2, and Condition 3, respectively. Each panel includes: ML transient responses after de-trapping (a,d,g), ML transient responses after trap-filling (b,e,h), and derived intensity of non-trap-controlled ML and trap-controlled ML (c,f,i). Note: in (c,f,i), the arrows and percentage characters indicate the ratio of trap-controlled ML intensity after two adjacent UV irradiations.

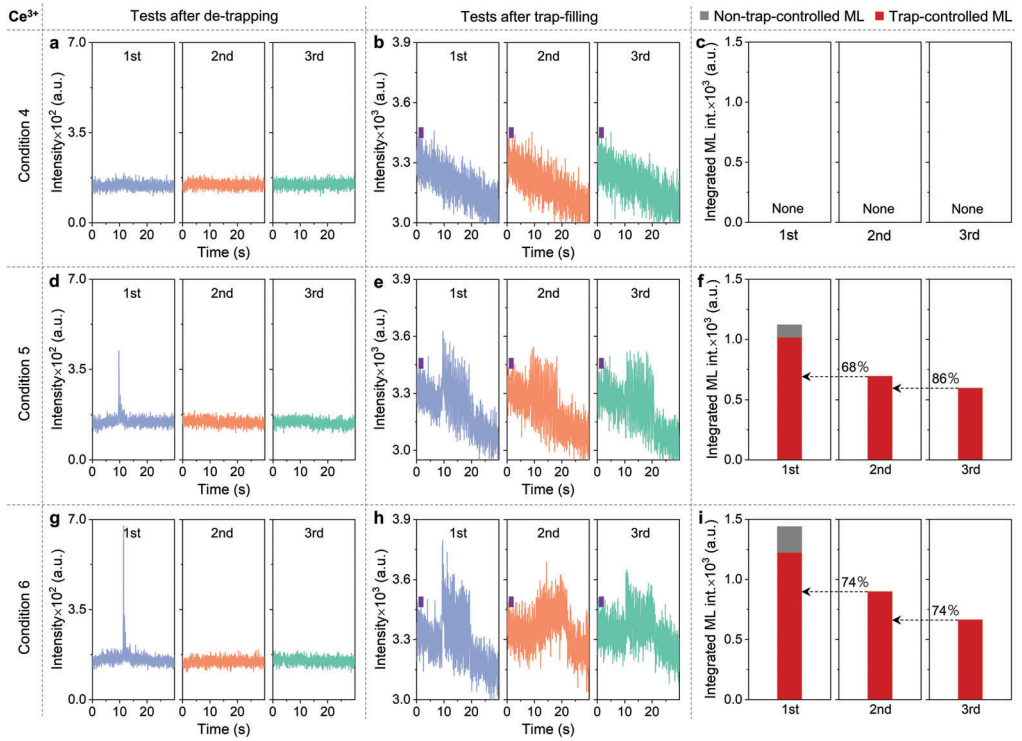

Figure 11. ML properties of CaZnOS:Ce^{3+} under cyclic friction tests for different conditions. Panels a–c), d–f), and g–i) correspond to compression–release tests conducted under Condition 4, Condition 5, and Condition 6, respectively. Each panel includes: ML transient responses after de-trapping (a,d,g), ML transient responses after trap-filling (b,e,h), and derived intensity of non-trap-controlled ML and trap-controlled ML (c,f,i). Note: in (c,f,i), the arrows and percentage characters indicate the ratio of trap-controlled ML intensity after two adjacent UV irradiations.

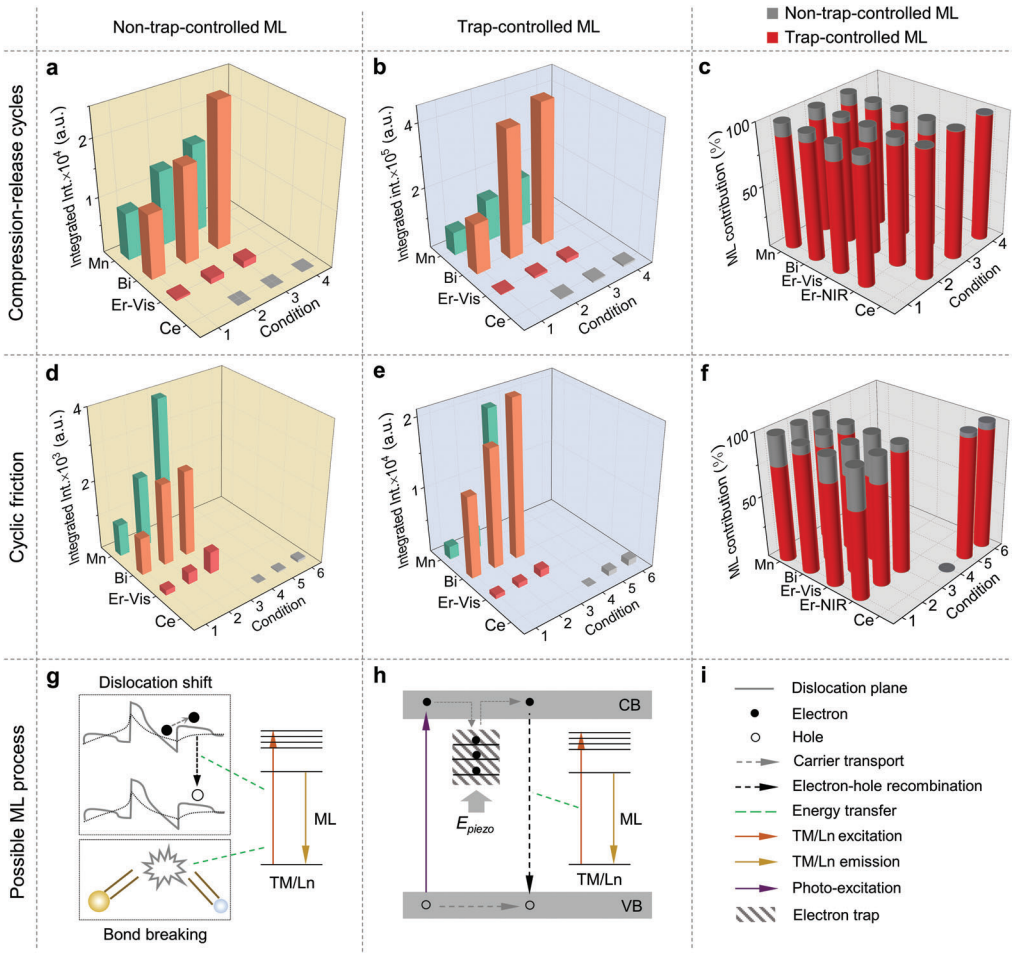

Figure 12. Comparison of non-trap-controlled ML and trap-controlled ML of four doped CaZnOS phosphors and potential ML origins. Panels a–c), and d–f) present ML properties observed during compression–release tests and cyclic friction tests, respectively. Each panel includes: average intensity of non-trap-controlled ML (a,d), average intensity of trap-controlled ML (b,e), and percentage contribution of non-trap-controlled ML and trap-controlled ML under different compression-release conditions (c,f). Panels g–i) illustrate the potential mechanisms for non-trap-controlled ML (g) and trap-controlled ML (h), while panel (i) provides related figure notes depicted in panels (g,h). Note that the top left of panel (g) illustrates plastic ML resulting from dislocation shift. The bottom left of panel (g) represents destructive ML arising from bond breaking and irreversible damage to the material.

high-temperature sintering process, wherein the reaction $Zn^{2+} + H_2 + O^{2-} \rightarrow Zn\uparrow + H_2O\uparrow$ occurs. The doped materials exhibit distinct ML spectra corresponding to the emission of the respective activators (Figure 1b and Table 1). CaZnOS:Mn^{2+} has a broad emission peaked at 620 nm from the $^4T_1(^4G)-^6A_1(^6S)$ transition of Mn^{2+}. CaZnOS:Bi^{3+} shows a broad emission peaked at 485 nm from the $^3P_{1,0}-^1S_0$ transition of Bi^{3+}. The ML spectra of CaZnOS:Er^{3+} are composed of visible and NIR emissions from the 4f–4f transition of Er^{3+}. CaZnOS:Ce^{3+} shows a broad emission (450–900 nm) from the 5d–4f transition of Ce^{3+}, with two peaks at 520 and 570 nm corresponding to the lowest 5d state to $^2F_{5/2}$ and $^2F_{7/2}$, respectively.[42] Notably, the ML of CaZnOS:Ce^{3+} is reported for the first time.

The doped CaZnOS phosphors displayed persistent luminescence after UV irradiation (Figure 1c). Thermoluminescent (ThL) measurements indicated the presence of carrier traps (Figure 1d). The evaluation of the trap depth shows a broadband distribution in these materials, ranging from 0.64 to 0.91 eV, suitable for producing persistent luminescence (Figure S2a, Supporting information,). CaZnOS:Bi^{3+} exhibited the most intense afterglow due to its higher trap concentration, while CaZnOS:Er^{3+} displayed the weakest afterglow intensity owing to the lowest trap concentration (Table 1). Moreover, these traps could be filled not only by UV irradiation but also by visible fluorescent lighting (Figure S2b, Supporting information). These results indicate the need to examine the ML properties of the four materials after evacuating the traps and filling them separately.

To evaluate the effectiveness of NIR laser de-trapping, NIR laser irradiation was applied on the doped CaZnOS phosphors. The disappearance of persistent luminescence and ThL signals indicated successful evacuation of the filled traps (Figure 1c,d). Subsequently, NIR laser irradiation was performed on CaZnOS-based ML composites, resulting in a complete disappearance of the afterglow curve (Figure S3, Supporting Information), which indicates effective removal of carriers from traps. Mechanical testing demonstrated that NIR laser irradiation had minimal

impact on the pressure load–time curve and frictional force–time curve of the ML composites (Figure 1e,f). In contrast, the conventional heat-treatment de-trapping method significantly affected the mechanical properties. The effectiveness of NIR laser de-trapping was attributed to the higher activation energy of ≈1.265 eV at 980 nm, which exceeded the trap depths of the materials. The insignificant thermal effect of NIR light, with a low optical power density of 260 mW cm^{-2}, ensured that the ML composites remained below 40 °C during the 10-min laser irradiation (Figure S4, Supporting Information), which is lower than the thermal curing temperature of the epoxy resin used (65 °C).

2.2. ML Properties of CaZnOS-Based Materials Under Cyclic Mechanical Stimulation

The ML properties of four CaZnOS-based materials were investigated under cyclic mechanical stimulation, including compression–release cycles and cyclic friction. The results of the ML spectra indicated that each doped CaZnOS phosphor displayed consistent profile and wavelength, independent of the type of mechanical stimulation or de-trapping and trap-filling conditions (Figure S5, Supporting Information). It suggests that the ML was derived from the characteristic emission of the doped ions. Various mechanical parameters within the range of previous reports were used in this work (**Table 2**; Table S2, Supporting Information). It was found that CaZnOS:Ce^{3+} required higher mechanical parameters to trigger ML, indicating a higher trigger threshold for this material compared to the other materials tested.

All four CaZnOS-based materials exhibited similar ML characteristics in compression–release cycles (**Figures 2–6**). All de-trapped materials exhibited non-trap-controlled ML, which gradually weakened under successive mechanical stimulation without self-recovery ability (as shown in a,d,g of Figures 2–6). Trap-controlled ML was observed in the materials subjected to trap-filling, but the ML intensity could not be fully recovered by post-UV irradiation (as shown in b,e,h of Figures 2–6). To determine the recovery degree of trap-controlled ML, the trap-controlled ML intensity was calculated by subtracting the afterglow background and the non-trap-controlled ML intensity from the total luminescence intensity of the trap-filled sample (Figure S6, Supporting Information). The calculation results showed that the recovery degree of trap-controlled ML ranged from 43% to 88% for the four materials. The panels c, f, and i of Figures 2–6 show the detailed data on the recovery degree of each material. Moreover, for each ML response of the trap-filled samples, the percentage of trap-controlled ML was consistently higher than that for non-trap-controlled ML, ranging from 64% to 100% for the former; and consistently, no more than 36% for the latter (Figure S7, Supporting Information).

Under cyclic friction, the ML behavior of the four materials showed similarities to that observed under compression–release cycles (**Figures 7–11**). Non-trap-controlled ML was detected in the de-trapped materials, with a gradual decrease in intensity over successive friction cycles (as shown in panels a, d, and g of Figures 7–11), without self-recovery ability. The trap-filled materials exhibited both trap-controlled and non-trap-controlled ML (as shown in panels b, e, and h of Figures 7–11), with the former being dominant and ranging from 54% to 100% for each group of ML response (Figure S8, Supporting Information). The recovery degree of trap-controlled ML by post-UV-irradiation varied from 3% to 86% for the four materials, without showing full recovery (as shown in panels c, f, and i of Figures 7–11).

2.3. Potential ML Mechanisms Involved in CaZnOS-Based Materials

To compare the ML properties of four doped CaZnOS materials, we conducted calculations to determine the average ML intensity and the relative ML contribution of non-trap-controlled ML and trap-controlled ML under different mechanical conditions (**Figure 12**a–f). The NIR ML intensity of CaZnOS:Er^{3+} is shown separately in Figure S9, Supporting Information, due to the use of different detectors, preventing direct comparison with visible ML intensity.

Under compression–release cycles and cyclic friction, we observed three main outcomes for the four materials. First, both intensity of non-trap-controlled ML and trap-controlled ML grown with the increase of the mechanical parameters for each doped CaZnOS materials. This behavior can be attributed to the input of more mechanical energy per unit time, resulting in more intense ML. Second, the intensities of non-trap-controlled ML and trap-controlled ML from CaZnOS:Mn^{2+} and CaZnOS:Bi^{3+} were significantly higher than those from CaZnOS:Er^{3+} and CaZnOS:Ce^{3+}. Among the four materials, CaZnOS:Bi^{3+} exhibited the highest trap-controlled ML, likely due to its higher trap density (Table 1). In contrast, CaZnOS:Ce^{3+} displayed the weakest ML regardless of the two types of ML, even when subjected to higher mechanical parameters than the other materials. We speculated that the weak ML in CaZnOS:Er^{3+} originated from the small absorption cross-sectional area and parity-forbidden 4f–4f transition of Er^{3+}.[16] The weakest ML in CaZnOS:Ce^{3+} may be attributed to the generation of Ce^{4+} (Figure S10, Supporting Information), which is typically known to suppress luminescence.[43,44] Third, the contribution of trap-controlled ML was much higher than that of non-trap-controlled ML (Figure S3, Supporting Information), ranging from 68.46% to 99.72% versus 0.28% to 31.54%, independent of the wavelength regions and the types and conditions of mechanical stimulation (Figure 12c,f). This finding indicates that the trap-controlled ML mechanism dominates the ML process. Notably, the percentage of non-trap-controlled ML in cyclic friction was higher than that that in compression–release cycles for each condition (Table S3, Supporting Information). This observation suggests that the two mechanical stimuli may elicit different responses from the CaZnOS host, resulting in varying percentages of non-trap-controlled ML, which will be discussed later.

The afore-mentioned findings indicate that the four CaZnOS-based materials are capable of emitting both non-trap-controlled and trap-controlled ML. However, the intensity of non-trap-controlled ML gradually diminishes under continuous mechanical stimulation and may eventually vanish completely. This type of ML does not exhibit the self-recovery property described in previous literature.[27] Hence, we can conclude that non-trap-controlled ML arises from irreversible changes in the lattice structure caused by mechanical stimulation, rather than

the previously reported piezophotonic effect that produces self-recoverable ML.[30–32] Considering the classification of ML,[2] we propose two possible explanations for non-trap-controlled ML in CaZnOS-based materials. The first possibility is plastic ML, where dislocation motion generates electrons that recombine with holes in the dislocation donor band, leading to ML (top of Figure 12g).[45,46] Shear stresses generated by frictional stimuli are more likely to induce dislocation slippage within the material,[47,48] which could account for the higher percentage of non-trap-controlled ML observed during cyclic friction compared to compression–release cycles. The second possibility is destructive ML, whereby energy released during the breaking of atomic and chemical bonds excites doped ions and generates ML (bottom of Figure 12g).[49] In addition, trap-controlled ML can be explained by the piezoelectricity-induced carrier de-trapping model (Figure 12h).[2] In this model, under optical excitation, electrons are excited to the valence band (VB) and subsequently trapped by electron traps, leaving holes in the conduction band (CB). The trapped carriers are then released from the traps due to the piezoelectric field, leading to nonradiative recombination with the holes. This process transfers energy to the doped ions, resulting in ML emission. The partial recovery of the trap-controlled ML might be attributed to plastic deformation and fracture of the crystal structure, causing the CaZnOS-based particles to lose their ability to trap electrons.

3. Conclusion

In conclusion, our study presents a comprehensive characterization strategy for investigating the ML properties of CaZnOS-based materials. Through a combination of NIR laser-assisted de-trapping, UV irradiation-induced trap-filling, in situ mechanical stimulation, and continuous recording of ML responses, we have successfully examined the ML behaviors of four doped CaZnOS materials (Mn^{2+}, Bi^{3+}, Er^{3+}, and Ce^{3+} ions) within the visible-NIR range. Our findings reveal important insights into the ML properties of these materials. The de-trapped materials exhibited non-trap-controlled ML, wherein the ML intensity gradually weakened under successive mechanical stimuli, without demonstrating any self-recovery property. In contrast, the trap-filled materials displayed ML properties that included both trap-controlled ML and non-trap-controlled ML, with the former being the dominant contributor to the overall ML intensity. Remarkably, the trap-controlled ML showed only partial recovery after trap filling. We attribute the non-trap-controlled ML to plastic ML and destructive ML phenomena, while the trap-controlled ML is explained by the piezoelectric-induced carrier de-trapping model. These findings not only clarify the conflicting reports regarding the generation and reproducibility of ML in CaZnOS-based materials but also provide deeper insights into the underlying ML mechanisms. Such insights can guide the future application of these materials, such as utilizing non-trap-controlled ML for structural health diagnosis and trap-controlled ML for repeatable stress distribution detection. Further, our developed characterization strategy holds significant value as a reference for establishing standardized protocols to evaluate the performance of a wider range of ML materials.

4. Experimental Section

Preparation of Phosphors and ML Composites: Phosphors with the chemical formulae $CaZn_{0.997}Mn_{0.003}OS$, $Ca_{0.94}Bi_{0.06}ZnOS$, $Ca_{0.96}Er_{0.04}ZnOS$, and $Ca_{0.995}Ce_{0.005}ZnOS$ were synthesized by a solid-state reaction method. The starting materials used were $CaCO_3$ (99.99%), ZnS (99.99%), $MnCO_3$ (99.95%), Bi_2O_3 (99.99%), Er_2O_3 (99.99%), CeF_3 (99.99%), and Li_2CO_3 (99.99%). To facilitate the reaction, a flux of Li_2CO_3 was added at a ratio of 6 wt%. The stoichiometric mixture of the respective phosphors was thoroughly ground and pressed into discs at a pressure of 10 MPa. The CaZnOS:Mn^{2+}, CaZnOS:Bi^{3+}, and CaZnOS:Er^{3+} phosphor discs were sintered in a horizontal tube furnace under an argon atmosphere at 1100 °C for 3 h. The CaZnOS:Ce^{3+} phosphor discs were sintered under a 5%H_2/95%N_2 reduction atmosphere at the same temperature and time. Following the sintering process, the resulting phosphor discs were pulverized, ground, and sieved through a 20 µm sieve, yielding microparticles of the desired phosphors. CaZnOS-based elastomer composites were prepared by incorporating the phosphor microparticles into an optical epoxy resin (SpeciFix, Struers GmbH) at a weight ratio of 1:9. The composites were prepared in disc-shaped molds with a diameter of 25 mm and a thickness of 15 mm.

Structural and Optical Characterization: XRD measurements were performed on an X-ray powder diffractometer (D8 Advance, Bruker AXS GmbH). XPS spectra were obtained using the K-Alpha X-ray photoelectron spectrometer system (Thermo Fisher Scientific). For the de-trapping purposes, a 980 nm continuous semiconductor laser (LD-60-5, Shandong Zhongke) with a fiber optic output and two plano-convex mirrors was utilized. The power output of the laser was set at 10 W by maintaining a constant current of 22 A, which provides a fixed average optical power density (260 mW cm^{-2}) on the samples. To fill the traps of phosphors, a handheld ultraviolet lamp (254 and 365 nm, 8 W) was employed. Afterglow curves were recorded using a fluorescence spectrometer (F-4700, Hitachi) equipped with a 150 W Xe lamp. ThL curves were measured using a ThL meter (FJ427A1, Beijing Nuclear Instrument Factory). Mechanical compression and friction experiments were performed using a universal testing machine (AGS-X, Shimadzu) and a friction testing machine (MS-T3001, Lanzhou Huahui), respectively. To analyze the ML spectra in the visible and NIR ranges, a QEPro spectrometer and a NIRQuest spectrometer (both from Ocean Optics) were employed, respectively. Detection of the ML signals was achieved using a visible photon-counting system (H10682-01, Hamamatsu Photonics) and an NIR photon-counting system (H10330C-75, Hamamatsu Photonics K.K.).

Supporting Information

Supporting Information is available from the Wiley Online Library or from the author.

Acknowledgements

This work was supported by the National Natural Science Foundation of China and its joint project with Guangdong Province (Nos. U22A20135 and 11774189), the Taishan Scholar Young Talent Program (No. tsqn202211057), the Natural Science Foundation of Shandong Province (No. ZR2023MA075), and the Fundamental Research Funds for the Central Universities.

Conflict of Interest

The authors declare no conflict of interest.

Data Availability Statement

The data that support the findings of this study are available from the corresponding author upon reasonable request.

Keywords

CaZnOS, mechanoluminescence, mechanoluminescent characterization, trap charging, trap discharging

Received: May 17, 2023
Revised: June 30, 2023
Published online: July 17, 2023

[1] G. Hong, *Science* **2020**, *369*, 638.
[2] J.-C. Zhang, X. Wang, G. Marriott, C.-N. Xu, *Prog. Mater. Sci.* **2019**, *103*, 678.
[3] B. Hou, L. Yi, C. Li, H. Zhao, R. Zhang, B. Zhou, X. Liu, *Nat. Electron.* **2022**, *5*, 682.
[4] X. Wu, X. Zhu, P. Chong, J. Liu, L. N. Andre, K. S. Ong, K. Brinson, A. I. Mahdi, J. Li, L. E. Fenno, H. Wang, G. Hong, *Proc. Natl. Acad. Sci. U. S. A.* **2019**, *116*, 26332.
[5] X. Ma, C. Wang, R. Wei, J. He, J. Li, X. Liu, F. Huang, S. Ge, J. Tao, Z. Yuan, P. Chen, D. Peng, C. Pan, *ACS Nano* **2022**, *16*, 2789.
[6] C. Li, Q. He, Y. Wang, Z. Wang, Z. Wang, R. Annapooranan, M. I. Latz, S. Cai, *Nat. Commun.* **2022**, *13*, 3914.
[7] X. Zhao, Z. Zhang, Q. Liao, X. Xun, F. Gao, L. Xu, Z. Kang, Y. Zhang, *Sci. Adv.* **2020**, *6*, eaba4294.
[8] X. Qian, Z. Cai, M. Su, F. Li, W. Fang, Y. Li, X. Zhou, Q. Li, X. Feng, W. Li, X. Hu, X. Wang, C. Pan, Y. Song, *Adv. Mater.* **2018**, *30*, 1800291.
[9] Y. Zhuang, X. Li, F. Lin, C. Chen, Z. Wu, H. Luo, L. Jin, R.-J. Xie, *Adv. Mater.* **2022**, *34*, 2202864.
[10] Y. Zhuang, R.-J. Xie, *Adv. Mater.* **2021**, *33*, 2005925.
[11] B. Chen, X. Zhang, F. Wang, *Acc. Mater. Res.* **2021**, *2*, 364.
[12] X. Zhang, J. Zhao, B. Chen, T. Sun, R. Ma, Y. Wang, H. Zhu, D. Peng, F. Wang, *Adv. Opt. Mater.* **2020**, *8*, 2000274.
[13] Y.-L. Yang, X.-C. Yang, J.-Y. Yuan, T. Li, Y.-T. Fan, L. Wang, Z. Deng, Q.-L. Li, D.-Y. Wan, J.-T. Zhao, Z.-J. Zhang, *Adv. Opt. Mater.* **2021**, *9*, 2100668.
[14] S. Zhou, Y. Cheng, J. Xu, H. Lin, W. Liang, Y. Wang, *Laser Photonics Rev.* **2022**, *16*, 2100666.
[15] X. Liu, P. Xiong, L. Li, M. Yang, M. Yang, C. Mao, *Mater. Horiz.* **2022**, *9*, 1658.
[16] J. Lei, W. Li, Y. Tang, Y. Cai, S. Wang, K. Dou, J.-C. Zhang, *J. Mater. Chem. C* **2023**, *11*, 3588.
[17] Y. Zhang, X. Zhang, H. Wang, Y. Tian, H. Pan, L. Zhang, F. Wang, J. Chang, *Adv. Funct. Mater.* **2021**, *31*, 2006357.
[18] Y. Ding, B. So, J. Cao, L. Wondraczek, *Adv. Sci.* **2022**, *9*, 2201631.
[19] L. Li, L. Wondraczek, L. Li, Y. Zhang, Y. Zhu, M. Peng, C. Mao, *ACS Appl. Mater. Interfaces* **2018**, *10*, 14509.
[20] M. Su, P. Li, S. Zheng, X. Wang, J. Shi, X. Sun, H.-W. Zhang, *J. Lumin.* **2020**, *217*, 116777.
[21] Y.-L. Yang, Q.-L. Li, X.-C. Yang, W. Yang, R. An, T. Li, Y. Zhou, H.-W. Zhang, J.-T. Zhao, Z.-J. Zhang, *J. Mater. Chem. C* **2020**, *8*, 3308.
[22] Y.-T. Fan, Y.-L. Yang, T. Li, J.-Y. Yuan, Q.-L. Li, J.-T. Zhao, D.-Y. Wan, Z.-J. Zhang, *J. Mater. Chem. C* **2021**, *9*, 5868.
[23] J. Jia, X. Gao, G. Zou, *Adv. Funct. Mater.* **2022**, *32*, 2207881.
[24] J.-C. Zhang, L.-Z. Zhao, Y.-Z. Long, H.-D. Zhang, B. Sun, W.-P. Han, X. Yan, X. Wang, *Chem. Mater.* **2015**, *27*, 7481.
[25] J.-Y. Yuan, Y.-L. Yang, X.-C. Yang, Y.-T. Fan, T. Li, M. Huang, F. Zhang, Q.-L. Li, J.-T. Zhao, Z.-J. Zhang, *J. Mater. Chem. C* **2021**, *9*, 7689.
[26] D. Tu, C.-N. Xu, Y. Fujio, A. Yoshida, *Light. Sci: Appl.* **2015**, *4*, e356.
[27] Y. Zhao, D. Peng, G. Bai, Y. Huang, S. Xu, J. Hao, *Adv. Funct. Mater.* **2021**, *31*, 2010265.
[28] Y. Du, Y. Jiang, T. Sun, J. Zhao, B. Huang, D. Peng, F. Wang, *Adv. Mater.* **2019**, *31*, 1807062.
[29] V. K. Chandra, B. P. Chandra, P. Jha, *Appl. Phys. Lett.* **2013**, *103*, 161113.
[30] H. Zhang, D. Peng, W. Wang, L. Dong, C. Pan, *J. Phys. Chem. C* **2015**, *119*, 28136.
[31] X. Wang, D. Peng, B. Huang, C. Pan, Z. Wang, *Nano Energy* **2019**, *55*, 389.
[32] L. Li, L. Wondraczek, M. Peng, Z. Ma, B. Zou, *Nano Energy* **2020**, *69*, 104413.
[33] J.-C. Zhang, N. Gao, L. Li, S. Wang, X. Shi, M. Sun, X. Yan, H.-W. He, X. Ning, B. Huang, J. Qiu, *Adv. Funct. Mater.* **2021**, *31*, 2100221.
[34] J.-C. Zhang, X.-Y. Xue, Y.-F. Zhu, S. Wang, H.-W. He, X. Yan, X. Ning, D. Wang, J. Qiu, *Chem. Eng. J.* **2021**, *406*, 126798.
[35] T. Jiang, Y.-F. Zhu, J.-C. Zhang, J. Zhu, M. Zhang, J. Qiu, *Adv. Funct. Mater.* **2019**, *29*, 1906068.
[36] J.-C. Zhang, C. Pan, Y.-F. Zhu, L.-Z. Zhao, H.-W. He, X. Liu, J. Qiu, *Adv. Mater.* **2018**, *30*, 1804644.
[37] J.-C. Zhang, X.-H. Fan, X. Yan, F. Xia, W. Kong, Y.-Z. Long, X. Wang, *Acta Mater.* **2018**, *152*, 148.
[38] X. Wang, Y. Chen, F. Liu, Z. Pan, *Nat. Commun.* **2020**, *11*, 2040.
[39] P. Pei, Y. Chen, C. Sun, Y. Fan, Y. Yang, X. Liu, L. Lu, M. Zhao, H. Zhang, D. Zhao, X. Liu, F. Zhang, *Nat. Nanotechnol.* **2021**, *16*, 1011.
[40] S. Huo, P. Song, B. Yu, S. Ran, V. S. Chevali, L. Liu, Z. Fang, H. Wang, *Prog. Polym. Sci.* **2021**, *114*, 101366.
[41] U. Eduok, O. Faye, J. Szpunar, *Prog. Org. Coat.* **2017**, *111*, 124.
[42] Z.-J. Zhang, A. Feng, X.-Y. Sun, K. Guo, Z.-Y. Man, J.-T. Zhao, *J. Alloys Compd.* **2014**, *592*, 73.
[43] A. Revaux, G. Dantelle, N. George, R. Seshadri, T. Gacoin, J.-P. Boilot, *Nanoscale* **2011**, *3*, 2015.
[44] M. M. Taniguchi, E. Silva, M. A. T. Silva, L. S. Herculano, R. F. Muniz, M. Sandrini, M. P. Belançon, *J. Non-Cryst. Solids* **2020**, *547*, 120307.
[45] B. P. Chandra, *Radiat. Eff. Defects Solids* **1996**, *138*, 119.
[46] M. V. Mukhina, J. Tresback, J. C. Ondry, A. Akey, A. P. Alivisatos, N. Kleckner, *ACS Nano* **2021**, *15*, 4115.
[47] H. Xie, C. He, *Int. J. Rock Mech. Min. Sci.* **2004**, *41*, 366.
[48] D. Li, Z. Sun, T. Xie, X. Li, P. G. Ranjith, *Eng. Geol.* **2017**, *228*, 270.
[49] A. J. Walton, *Adv. Phys.* **1977**, *26*, 887.